TECHNOLOGY FOR FABRICATING DENSE 3-D MICROSTRUCTURE ARRAYS FOR BIOMIMETIC HAIR-LIKE SENSORS

Y. Tang, R. L. Peterson, and K. Najafi
Center for Wireless Integrated MicroSensing and Systems (WIMS^2)
University of Michigan, Ann Arbor, MI, USA

ABSTRACT

This paper reports high-density arrays of 3-dimensional (3-D) high-aspect ratio MEMS structures that can imitate biological hairs. Hair has many properties, including high aspect ratio (long and small footprint), large surface area, mechanical flexibility and robustness, and customized material properties. Hair sensors can be made in large arrays, provide high sensitivity through local neural processing, and offer a multiplicity of functions. In nature, hairs typically exist in large-scale arrays, offering distributed sensing functions, redundancy, and improved stability, sensitivity, and dynamic range. In this paper, we present a fabrication technology for forming highly dense 3-D arrays of microstructures useful for a variety of sensing applications, which realize some of these biological advantages. We have fabricated 4x4, 5x5, and 10x10 accelerometer arrays, achieving a sensor density of ~100 sensors/mm^2. Initial testing shows accelerometer resonant frequencies and static capacitance values that vary with proof mass and hair/spring dimensions as expected.

INTRODUCTION

One of the many approaches to develop sensors with improved performance, smaller size and enhanced functionality is based on biomimetic structures. Among them, hair-like structures are used extensively to achieve a myriad of functions including: flow sensing, temperature sensing, vibration sensing, etc. Biomimetic hair sensors offer a number of attractive features by combining mechanical sensing, local chemo-electric transduction, and sophisticated signal processing.

Our group has proposed the basic elements of a highly functional, sensitive and selective hair sensor structure as shown in Figure 1 [1]. These elements are: 1) the core hair-like structure, 2) the transduction mechanism, 3) local interface circuits, and 4) signal processing and control electronics for the array.

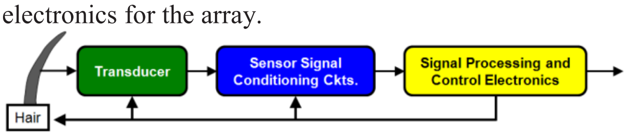

Figure 1: Biomimetic hair sensor structure [1].

The hair structure offers numerous advantages [1]. It is tall in the third dimension thus enabling a very small footprint and excellent spatial resolution. Due to the small footprint of each individual hair, arrays of them can be used to enhance sensitivity and selectivity (Figure 2a). Furthermore, individual hair structures can potentially be mechanically coupled to add new functionality (Figure 2b). The transduction mechanism that converts external parameters to electrical signals can take many different forms. If small electrical output signals can be processed at the site of each hair sensor element with local circuitry (Figure 2a), the effect of parasitics can be greatly reduced. We refer to the hair sensor and its local circuitry as a "hexel". The hair geometry and material can be tailored for various applications and performance requirements (Figure 2c). In addition, the substrate material can be flexible to conform to different surface topology (Figure 2d).

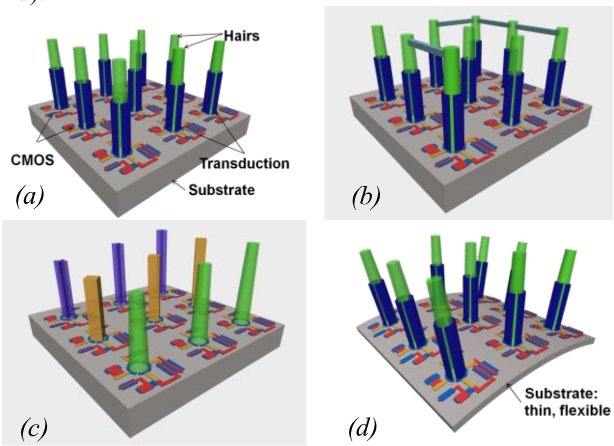

Figure 2: Schematics of possible aspects of hair-like arrays: (a) 3-D hair array with transduction and local interface circuitry; (b) mechanically-interconnected hairs within an array; (c) different hairs within the array; (d) hair array on a flexible substrate.

Previous works on biomimetic hair-like sensors required separate assembly processes for the hair and transducer [2-4]. Our group has reported two different hair-based air flow sensors. The more recent approach has a hair-like post to convert the drag force to pressure and uses microhydraulic structure for hydraulic amplification of the signal and capacitive transduction [5].

In this work, we report a representative fabrication technology to form a large array of sensors (i.e., accelerometers) and demonstrate the ability to achieve all of the basic features of hair-sensor structures: 1) long and small foot-print hair-like structures; 2) mechanical structures consisting of a proof mass and a flexible support spring formed normal (i.e., vertical) to the plane of the wafer (instead of parallel to the plane of the wafer); 3) dense arrays; and 4) built-in transduction mechanisms (e.g., capacitive) (Figure 3a). Each sensor (Figure 3b) consists of a proof mass atop a narrow post. The post acts as mechanical spring and the mass is surrounded by four walls for capacitive sensing of deflection.

DEVICE DESIGN

Critical parameters in the aforementioned 2-axis acceleration sensor array include: total height, mass size, hair cross-section area, capacitive sensing gaps and the

978-1-4673-5655-8/13/$31.00 ©2013 IEEE

number of hairs in the array. We use the *Solid Mechanics* module coupled with the *Electrostatics* module in COMSOL to simulate the spring constant, resonant frequency and sensitivity of sensor arrays with different design parameters. Figure 4 shows the displacement field and the stress distribution along the post. Using DRIE lag, the long post and proof mass are defined simultaneously in the vertical direction. Thus the length of the post and height of the mass are of the same order of magnitude. A longer or narrower post produces a more compliant spring; mass sizes can be tuned to produce the desired sensitivity.

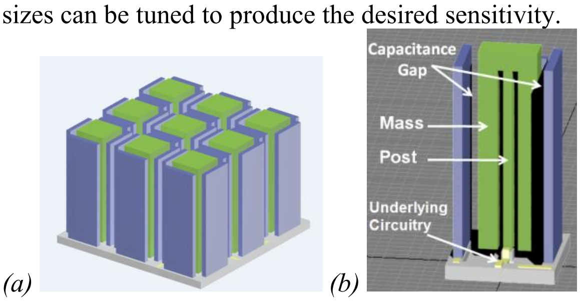

Figure 3: 3-D hair sensor arrays for acceleration sensing. (a) Array of hair sensors. (b) Cross sectional view of single hair sensor showing the support post (spring), mass and capacitive gaps to walls.

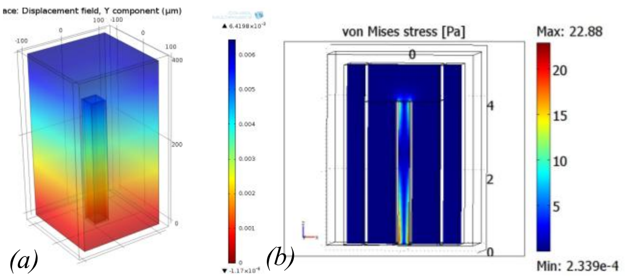

Figure 4: (a) Surface displacement profile of a single hair. (b)Von Mises stress distribution when the hair is deflected.

Table 1: Measured vs. simulated resonant frequencies (in kHz) for different mass and post sizes for 5x5 arrays.

Mass ⇓	**Post Size ⇒**	$30^2 \mu m^2$	$40^2 \mu m^2$	$50^2 \mu m^2$
400μm	Simulated	15.76	27.85	43.13
square	Measured	~16.5	~27.6	~41.5
500μm	Simulated	12.57	22.29	34.55
square	Measured	~11.7	~20.6	~32.6

Table 1 lists the simulated resonant frequencies for the first bending mode. A smaller post (i.e., a smaller bond area) leads to more compliant springs, while a larger mass decreases the resonant frequency. The mass footprints range from 200 x 200 μm^2 to 500 x 500 μm^2. The capacitive gap is swept from 0.5 µm to 7.5 µm. The array sizes are chosen to obtain total sensitivity around 0.5 fF/g. Figure 5a shows the sensitivity of 10 x 10 arrays vs. hair diameter for a 300-µm high post and 400-µm high mass assuming a sensing gap of 7.5 µm. The sensitivity of a single hair can be greatly increased by reducing this gap below 1 µm (Figure 5b). If the gap is reduced below a micron, the sensitivity of a single hair would be comparable to that of a 10 x 10 array with a 7.5 µm gap. The gap could be reduced by minimizing the amount of undercut in the DRIE, or by partially filling the sensing trench (e.g., with polysilicon).

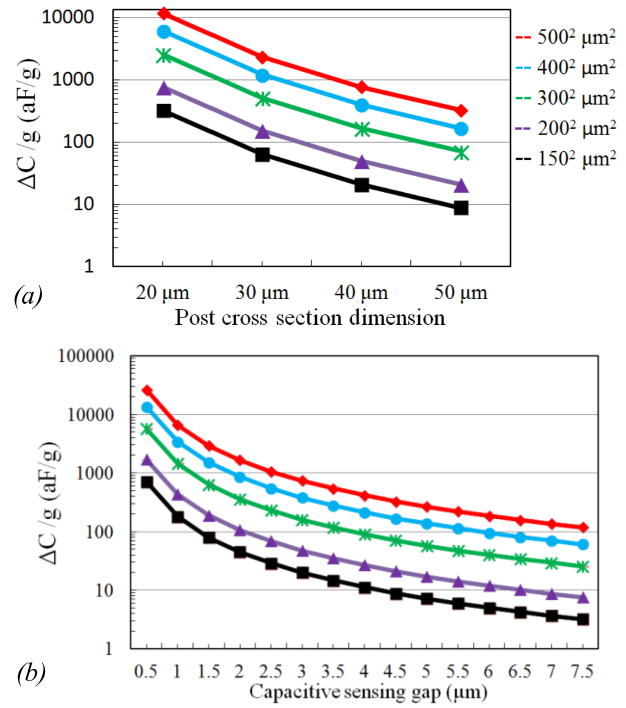

Figure 5: (a) Sensitivity of 10 x 10 arrays vs. hair diameter for a 300-µm high post and 400-µm high mass (b) Sensitivity of a single hair vs. gap for a 20 µm post.

FABRICATION PROCESS

The prototype sensor array is fabricated using a silicon-on-glass (SOG) process (Figure 6). The process starts with a blank double side polished 500 µm, 0.005-0.020 Ohm-cm, p-type silicon wafer. A shallow recess of 2 µm is patterned in the silicon wafer using DRIE. A long DRIE step is then used to define the small capacitive gaps and the gap between the post and the mass, while simultaneously etching more deeply to separate neighboring sensors by exploiting aspect ratio dependent etching (RIE lag). A recess is etched in a Pyrex 7740 wafer to create the bond pads. Two metal layers are patterned on the glass wafer. The first layer (Ti/Pt of 200 Å /1300 Å) is for metal interconnects in direct contact with the silicon posts. The second optional stack consists of Ti/Al of thickness 200 Å /1500 Å that may protect the first metal layer from being sputtered during final DRIE step. The Si and glass wafers are anodically bonded. The bonded wafers are flipped and dry etched from the silicon side to release the mass.

High Aspect Ratio DRIE

High aspect ratio DRIE is critical in defining the capacitive sensing gap, the mass/post dimension, and the separation between sensing elements in the array. Our group previously developed an improved DRIE process for ultra high aspect ratio silicon trenches with reduced undercut [6]. This is accomplished by ramping process pressure, etch power, and switching time. An aspect ratio of 70 was achieved for a 400 µm deep trench with 5.7 µm average gap, and 300 µm deep trench for 3 µm gap. The first depth corresponds to the mass height while the latter is the spring length. The separation between neighboring electrodes is >10 µm to prevent capacitive feed-through.

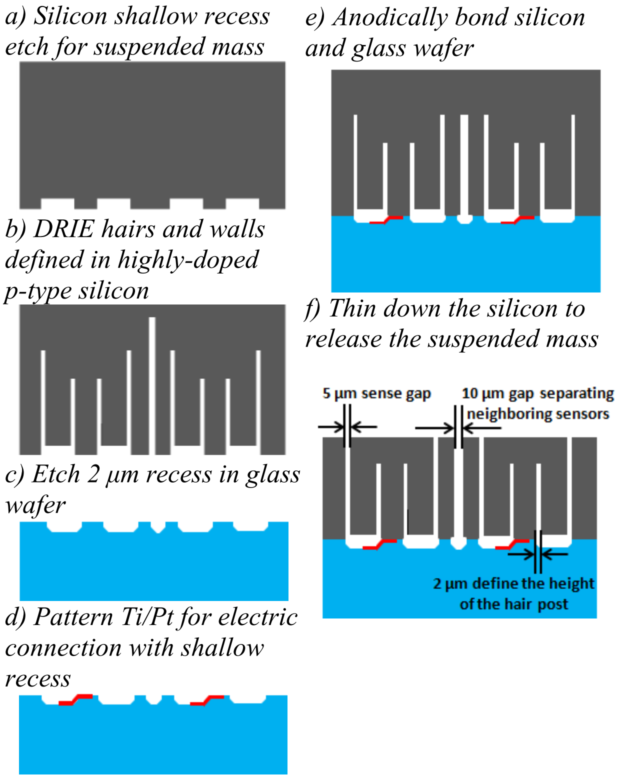

Figure 6: Silicon-on-Glass (SOG) Fabrication Process

Anodic Bonding with Small Post Area

In order to increase sensitivity, we should reduce the cross-sectional area of the hair post to make the spring more compliant. Anodic bonding is chosen for its high bond strength and simplicity but it requires a minimum surface area for a successful bond. To minimize the post area, we use pre-bond cleaning and plasma activation of wafer surfaces, good bond alignment, and optimize the bonding voltage, temperature, and annealing process.

For Si wafer pre-cleaning, H_2SO_4–H_2O_2 (1:1 Piranha) and HF cleaning can be used to significantly enhance the bonding strength. In our case Piranha is necessary because polymers such as photoresist and CF_6-induced compounds can stick to the walls of the deep trenches during DRIE. Piranha clean of the silicon wafer along with acetone clean of the glass wafer results in almost 100% yield for posts with cross-sections larger than 30 μm x 30 μm. Oxygen plasma activation is also used to treat both wafers before bonding. For both silicon and glass surfaces, the total surface energy increases even at low power or short plasma exposure times. We pre-bond by applying -500V at 250 °C for 30 minutes. Then we perform the second bonding step by applying -1300V at 350 °C. After the second bonding is complete, we anneal the wafers at 350 °C for 1.5 hours and slowly ramp down to room temperature over 2 hours.

The bond success is assessed visually. The darker color in Figure 7a indicates well-bonded areas while the light colored areas represent the recess in the glass. There are no visible particles at the interface. On top of each post (Figure 7b) is a small piece of broken glass, indicating a strong bond. A close-up of the cross-section of a sensing cell interface is shown in Figure 7c.

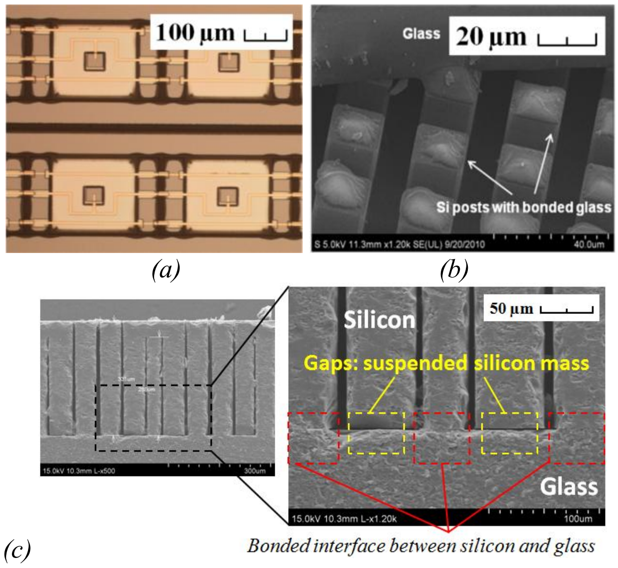

Figure 7: Bonded silicon-glass interface: (a) Grey color indicates good-quality bonding with metal; (b) 20x20 μm^2 silicon posts after fracture; (c) SEM of hair structure cross-section and close-up of the silicon-glass interface.

Electrical Connections

The metal layers in between the bonded silicon post and glass island allow probing of the sensors' static capacitance and dynamic response. However because the metal layers lie at the bond interface, they require careful design to obtain a high-quality bond. Based on experiments varying the thickness of the exposed metal from 300 Å to 700 Å, we conclude that for the smallest successful bonding area of 20 μm x 20 μm, the metal stack should not be more than 500 Å higher than the glass surface. A thicker metal stack means that the wafers cannot be successfully bonded. However, a thin metal layer can cause its own processing problems. If the lines are sputtered during the release DRIE step or coated with CF_6, the metal connections can be damaged. Additionally, traces made in such a thin layer will have relatively high resistance. To address these problems, using the same electrode mask, we etch a shallow glass recess (> 1200 Å) directly under the metal lines. This allows deposition of a thicker layer of metal that barely breaches the surface to contact the bonded silicon.

Figure 8 shows SEM photographs of a 10x10 accelerometer array diced to expose the cross-section of the capacitive walls, proof mass and the underlying electrical connections.

TESTING RESULTS

Static Measurement

To effectively read out large sensor arrays, for this preliminary implementation we connect all devices in parallel to achieve greater sensitivity and measure the static capacitance using an HP 4284A LCR Meter at 1 kHz. The maximum sensor density realized is high, ~100 sensors/mm^2. Figure 9 compares experimental and simulated values of static capacitance for both 400 x 400 μm^2 and 500 x 500 μm^2 mass arrays. The static capacitance scales almost linearly with array size. The capacitive sensing gap varies from 5 μm to 7.5 μm, on

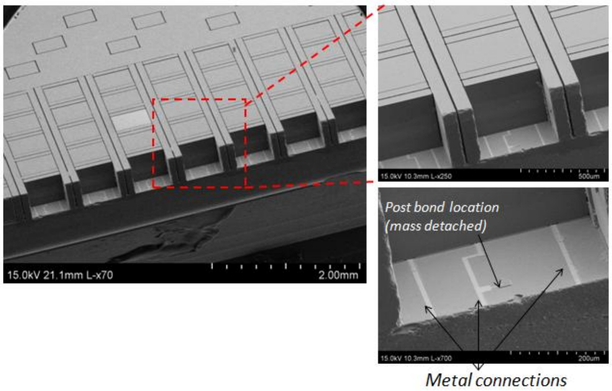

Figure 8: SEM photographs of a 10x10 accelerometer array diced to expose the cross-section of the capacitive walls, proof mass and the underlying electrical connections.

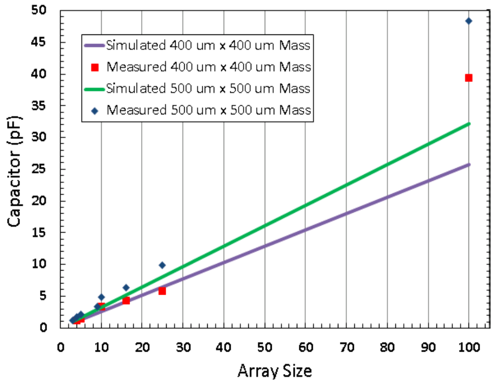

Figure 9: Static capacitance measurement compared with simulated values assuming an average capacitive gap of 5.5 µm for 400 µm x 400 µm and 500 µm x 500 µm mass.

average, across the fabricated wafers. This variation accounts for differences in the capacitance of the same nominal array at different locations. The measured capacitance values are generally slightly higher than simulated values, due to parasitic capacitance from the pads and between metals and ground.

Resonant Measurement

The frequency response of the sensor array is measured using a standard bias-drive-sense method [7]. A DC bias applied to the proof mass creates a force which softens the spring, decreasing the vibration resonant frequency of the hair mass/post. An AC signal is applied to one electrode and the resulting signal is picked at the other side, 180˚ offset. A typical frequency response of a $400^2\mu m^2$ mass - $30^2\mu m^2$ post array is shown in Figure 10. The multiple peaks may be due to variation in mass/post dimensions across the array. The measured resonant frequencies are compared to simulated values in Table 1.

SUMMARY

By taking advantage of high aspect ratio DRIE and SOG process, we fabricate a new class of highly dense 3-D MEMS sensor arrays which may offer improvements in performance, robustness, and multi-sensor functionality. We implement 2-axis acceleration sensor arrays using this technology.

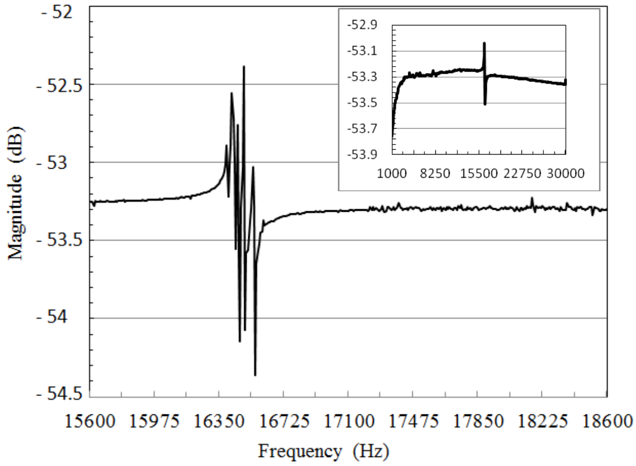

Figure 10: Frequency response of a $400^2\mu m^2$ mass / $30^2\mu m^2$ 5x5 array.

ACKNOWLEDGEMENTS

This project is funded by the Micro Autonomous Systems & Technology (MAST) Program of the Army Research Lab (ARL) under Award Number W911NF-08-2-0004. This work was performed at the Lurie Nanofabrication Facility, a member of the National Nanotechnology Infrastructure Network, which is supported in part by the National Science Foundation.

REFERENCES

[1] K. Najafi, "Biomimetic Hair Sensors: Utilizing the Third Dimension", in *Proc. IEEE Sensors Conf.*, Taipei, Oct. 2012.

[2] R. K. Jaganatharaja, *et al.*, "Highly-sensitive, Biomimetic Hair Sensor Arrays for Sensing Low-frequency Air Flows", in *Transducers'09*, Denver, USA, June 21-25, 2009, pp. 1541–1544.

[3] Y. Ozaki, T. Ohyama, *et al.*, "An Air Flow Sensor Modeled on Wind Receptor Hairs of Insects", in *MEMS'00*, Miyazaki, Japan, January 23-27, 2000, pp. 531–536.

[4] N. Chen, *et al.*, "Design and Characterization of Artificial Haircell Sensor for Flow Sensing with Ultrahigh Velocity and Angular Sensitivity", *J. Microelectromech. Syst.,* vol.16, no. 5, pp. 999–1014, 2007.

[5] M. M. Sadeghi, R. L. Peterson, K. Najafi, "Micro-hydraulic Structure for High Performance Bio-mimetic Air Flow Sensor Arrays", in *IEDM'11*, Washington D.C, USA, 2011, pp. 673-676.

[6] K. J. Owen, R. L. Peterson, K. Najafi, "High Aspect Ratio Deep Silicon Etching", in *MEMS'12*, Paris, France, 2012, pp. 251-254.

[7] A. A. Trusov, A. M. Shkel, "Capacitive Detection in Resonant MEMS with Arbitrary Amplitude of Motion", *J. Microelectromech. Syst.,* vol.17, no. 8, pp. 1583–1592, 2007.

CONTACT

*K.Najafi, tel: +1-734-763-6650; najafi@umich.edu